Engineering Structures 53 (2013) 10–24

Contents lists available at SciVerse ScienceDirect

Engineering Structures

journal homepage: www.elsevier.com/locate/engstruct

Influence of modeling parameters on the response of degrading systems to near-field ground motions

Vicky Dimakopoulou [a], Michalis Fragiadakis [b], Constantine Spyrakos [a,*]

[a] Laboratory for Earthquake Engineering, National Technical University of Athens (NTUA), Iroon Polytechniou 9, 15780 Zografou, Greece
[b] Department of Civil and Environmental Engineering, University of Cyprus, P.O. Box 20537, 1678 Nicosia, Cyprus

ARTICLE INFO

Article history:
Received 14 May 2012
Revised 4 March 2013
Accepted 5 March 2013
Available online 29 April 2013

Keywords:
Near-field records
Forward directivity
Degrading systems
Single and multi-degree-of-freedom systems
Inelastic displacement ratio

ABSTRACT

The influence of modeling assumptions on the seismic response of structures subjected to near-field ground motions is investigated. Emphasis is given on degrading systems, since real-world structures do not have infinite displacement capacity as many inelastic models assume, while such systems are able to explicitly take into consideration the effect of stiffness and strength degradation. Near-field ground motions are of particular interest, since, compared to far-field records, may cause increased demand caused by the velocity pulse in their fault-normal component. Single-degree-of-freedom (SDOF) oscillators with generic multilinear force–deformation backbones are first considered in order to derive general conclusions for a wide range of periods. The effect of every parameter that describes the backbone is studied separately in order to identify the sensitivity of the demand when the system is subjected to pulse-like ground motions. Moreover, a nine-story steel moment resisting frame is studied in order to show that the observations made on SDOF structures extend to multi-degree-of-freedom buildings.

1. Introduction

Near-field ground motions with forward directivity are characterized by strong, coherent, long-period pulses. These properties differentiate the structural response compared to that of non-pulse like ground motions. The special characteristics of near-field, forward directivity ground motions are directly correlated with the magnitude, the source type and the direction of rupture propagation relative to the site. Among the first to note that near-field records that contain strong velocity pulses may produce increased demand were Bertero et al. [1]. Over the years, many studies (e.g. [2–5]) have confirmed that structures located in the near-field zone may experience increased inelastic behavior caused by the velocity pulse in the fault-normal component of the ground motion.

The influence of modeling assumptions on structures subjected to pulse-like ground motions is investigated placing emphasis on systems with degrading properties. Degradation can be distinguished to "in-cycle" and to "cyclic" degradation. The first one is observed under monotonic loading and is attributed to the properties of member force–deformation (or moment–rotation) backbone, while the second is due to the deterioration of the building's capacity caused by cyclic loading. For example, first-mode dominated structures may be approximated with SDOF systems with a bilinear capacity curve that may be elastic-perfectly plastic or may exhibit some strain-hardening. This assumption leads to an erroneous estimation of the demand, since, in the actual case, the system capacity degrades after some deformation instead of remaining constant (or gradually increasing) as a bilinear model would predict. However, this simplification is quite common since it is sufficient for elastic and early inelastic limit-states. Moreover, often the inelastic response of buildings is modeled assuming a bilinear moment–rotation relationship for the plastic hinges. Similarly, when fiber models are used, the existence of steel fibers that follow a bilinear stress–strain relationship does not actually allow the cross-section capacity to degrade. The significance of modeling the degradation is shown in Fig. 1. Fig. 1a shows the capacity curve of a nine-story steel plane frame with and without degradation, while Fig. 1b shows the corresponding moment–rotation relationships. Different modeling of the member (or connection) properties will result in significant differences in the building capacity curve and seismic response.

The objective of this work is to investigate the inelastic response of degrading single- and multi-degree-of-freedom systems when subjected to the forward-directivity component of near-field ground motions. To cover a wide range of possible structures we first study single degree-of-freedom (SDOF) structures with multilinear degrading backbones and we attempt to draw useful conclusions regarding the effect of every parameter that describes the backbone of these systems as a function of the seismic intensity.

* Corresponding author. Tel.: +30 6944330266.
E-mail addresses: vdimak@central.ntua.gr (V. Dimakopoulou), mfrag@ucy.ac.cy (M. Fragiadakis), cspyrakos@central.ntua.gr (C. Spyrakos).

0141-0296/$ - see front matter © 2013 Elsevier Ltd. All rights reserved.
http://dx.doi.org/10.1016/j.engstruct.2013.03.008

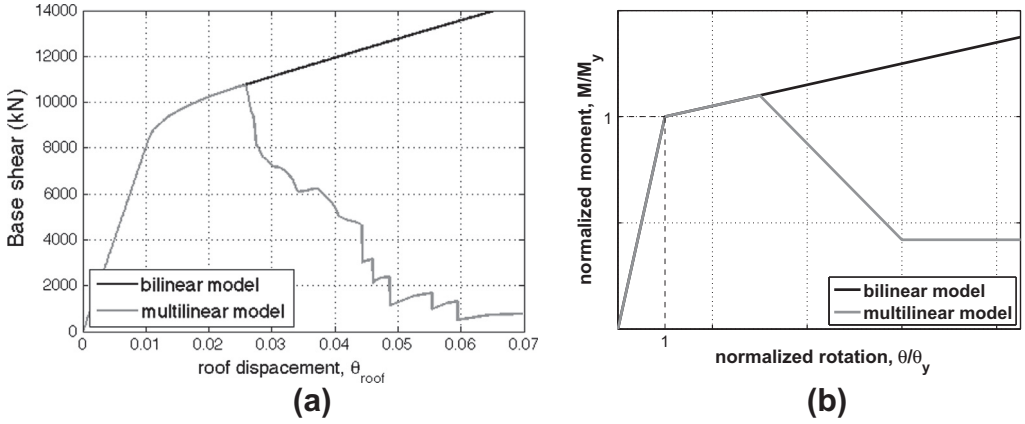

Fig. 1. (a) Static pushover curves of a nine-story steel frame using bilinear and multilinear moment–rotation relationships and (b) a typical moment–rotation relationship.

At a second stage, we extend the discussion to a real-scale steel building.

2. Single-degree-of-freedom systems

A wide range of single-degree-of-freedom (SDOF) oscillators is studied. The systems are modeled having a multilinear backbone, as shown in Fig. 2. This modeling allows the in-cycle degradation, i.e. degradation of the monotonic envelope, and consists of four branches. The first branch is linear elastic and is followed by a hardening branch that terminates at a "capping-point". The "capping-point" marks the beginning of a degrading branch with negative stiffness/slope. A very steep slope indicates fracturing, while a mild slope combined with a longer post-elastic segment, corresponds to a more ductile system. The descending segment terminates at a residual plateau thus resulting to a quadrilinear model. Discussion on this modeling and its application to the hysteretic response of structural members can be found in a number of publications, i.e. [6–8]. In the present investigation a bilinear oscillator for comparison reasons is also considered. Unless otherwise stated, the monotonic backbone of the bilinear oscillators are characterized by an elastic and a hardening branch, with slopes equal to those of the multilinear system they are compared with.

According to the notation of Fig. 2, the first branch is elastic with stiffness a_{el} followed by a post-yield hardening branch with slope a_h. Note that all slope quantities are defined as fractions of the elastic slope a_{el}. The hardening branch terminates at the "capping" point indicating ductility μ_c. The third branch has negative stiffness equal to $-a_c$ and terminates at a horizontal plateau with normalized capacity r, that denotes the residual capacity. The residual capacity r is defined as fraction of the yield force. Therefore, the monotonic backbone of the quadrilinear model is fully described by six parameters: the elastic slope (a_{el}) and the yield strength (F^{yield}), used also for the bilinear case, and by the a_h, a_c, μ_c and r as discussed above. A seventh parameter that may be introduced in this modeling is the ultimate ductility μ_f, shown in Fig. 2 with a vertical dashed line. This parameter marks the total failure of the system and can be used to abruptly drop the system capacity to zero after some deformation. μ_f is not considered in all analyses prior to Section 4.3.5 of this work. Moreover, although, the study places emphasis on the monotonic in-cycle degradation, the influence of the hysteretic parameters is also discussed.

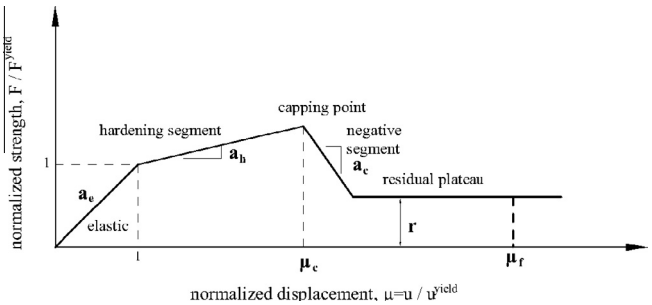

Fig. 2. The force–displacement relationship of the oscillator.

Different combinations of the six parameters that characterize the SDOF oscillators are able to describe a wide variety of structural systems. For example, according to the parameters adopted in Ref. [7], Fig. 3a and b corresponds to a reinforced concrete specimen and a steel specimen, respectively. The adopted modeling can simulate both ductile and brittle systems with either sudden or a gradual post-capping slope. Moreover, the modeling of Fig. 2 can be used at both the member and the global level. Using such modeling at the global level, allows approximation of the static pushover curve of a building [9]. Experimental tests are usually available only at the member level, i.e. cyclic tests of beams or columns [8]. Therefore, when this modeling is adopted for equivalent SDOF models of buildings, the parameters that describe the SDOF should be representative of the cyclic response of the buildings and, thus, can be obtained using appropriate numerical models only.

The SDOF system shown in Fig. 3c is used as the "reference", or "base-case", model throughout this study. This model is considered representative of many South European medium-rise RC buildings and has the following properties: $a_h = 5\%$, $\mu_c = 2$, $a_c = -50\%$, $r = 20\%$. A typical value equal to 5% was assigned to a_h, while $a_c = -50\%$ indicates a significant post-capping strength deterioration. Moreover, $\mu_c = 2$ indicates that the reference system chosen has rather small ductility capacity, while a low residual capacity of $r = 20\%$ was chosen corresponding to systems with poor detailing against large inelastic displacements. When results using a bilinear system are shown, the kinematic hardening is assumed equal to 5%, thus equal to the slope (a_h) of the reference system.

Throughout the study the backbone parameters are varied considering values that often appear in the literature when modeling steel or reinforced concrete buildings. More specifically, Chopra and Chintanapakdee [4] report that the dispersion in the response of bilinear oscillators is practically independent of the post-yield stiffness ratio a_h and assume $a_h = 3\%$. Following their findings, we impose a large variation on this parameter, assuming upper and lower values equal to 0% and 25%, in order examine its actual effect on the demand. Moreover, when we investigate the post-capping slope a_c, we assume $a_c = -0.1$, -0.5 and -2. Ibarra and Krawinkler

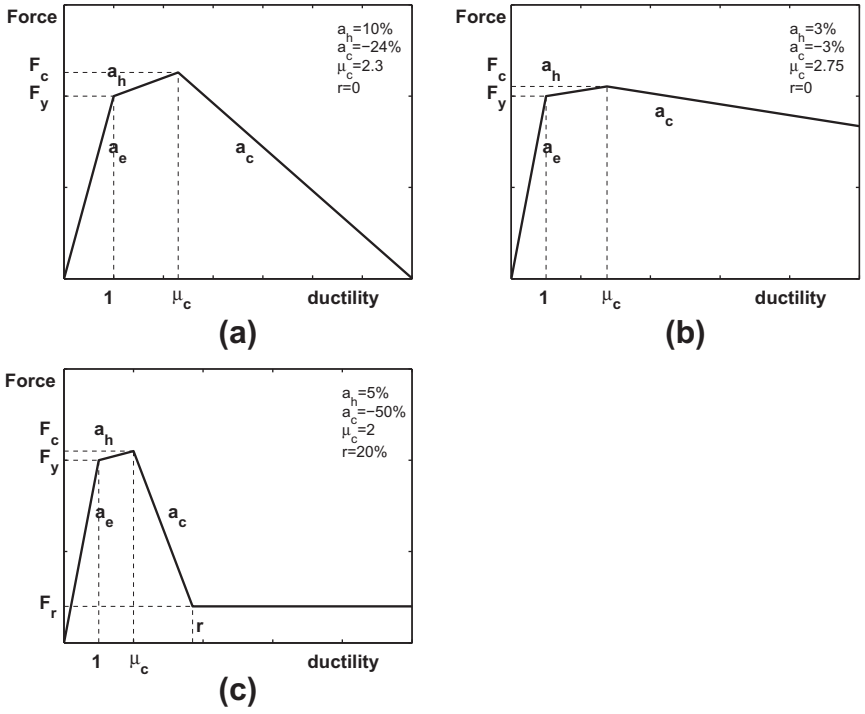

Fig. 3. (a) Reinforced concrete specimen, (b) steel specimen and (c) reference oscillator.

[6] suggest $a_c = -0.1$, -0.3, and -0.5 as small, large and very large a_c values, respectively. This assumption is also confirmed by the experimental data of other researchers [10–12]. Moreover, there are researchers, e.g. Haselton and Deierlein [13], who consider $a_c = -0.3$ for RC structures. In our study, we choose higher values beyond -50%, in order to investigate the effect of this parameter for non-ductile systems, representing the majority of buildings in Southern Europe. Following the same reasoning, the base case value of the post-capping ductility μ_c was set equal to 2, a rather small value for non-ductile structures, while the upper and lower thresholds were selected equal to 1.2 and 6, according to the literature [6,10–12]. Thus, all parameters selected are based on an extensive study of the literature. Finally, the cyclic response is based on the "hysteric material" available in the material library of the OpenSees software [14]. The force and displacement pinching parameters of the model are set equal to a moderate value throughout the paper. The effect of the cyclic parameters is investigated in Section 4.4.

3. Ground motion records

A set of 40 strong ground motion records, recorded normal to the fault trace and a set of 44 far-field records were used throughout the study. The near-field set and the properties of its records are listed in Table 1. The records correspond to events of magnitudes between 5 M_w and 7.6 M_w and were recorded on different soil types and distances from the rupture plane. Large variation among the records is observed with respect to the pulse duration and the pulse period. The predominant pulse periods T_p of Table 1 were taken from the PEER-NGA database, while this issue is identified and thoroughly discussed in the manual of the PEER NGA database, available from the PEER NGA website. The far-field set is that of the FEMA P-695 document. The FEMA P-695 [15] set includes earthquakes of magnitudes that exceed 6.5 M_w and have been recorded on soil types *C* and *D* following the NEHRP classification.

4. Parametric investigation

The concept of the inelastic displacement ratio, *C*, is adopted in order to study the effect of near-field ground motions. The inelastic displacement ratio is the maximum, over the entire response history, inelastic displacement demand, u_m, divided by the corresponding maximum elastic displacement demand, u_{el}. Thus, *C* is given by the following expression:

$$C = \frac{u_m}{u_{el}} = \frac{\mu}{R_y} \tag{1}$$

In order to compute *C* systems with given demand R_y have been used, where R_y is the strength reduction factor, that equal to the ratio of the $\zeta\%$-damped spectral acceleration demand $S_a(T_1,\zeta)$ times the system mass over the corresponding yield force. The inelastic displacement ratio for such systems is thus denoted as C_R. Such a notation is used in order to distinguish C_R from the case in which the inelastic displacement ratio is calculated using systems with constant ductility. Compared to the constant-ductility case, C_R has the advantage that its calculation does not require an iterative process and thus is more simple and robust. In general, C_R tends to infinity for systems with very short periods and to one after a limiting spectral period value that depends on the soil type, the input excitation and modeling [16].

If the strength reduction factor *R* is equal to $R = f_{el}/f_y = ku_{el}/ku_y = u_{el}/u_y$ and the inelastic displacement u_m is equal to μu_y, then it is easy to demonstrate that C_R is equal to the ratio μ/R_y, as also denoted in Eq. (1). Therefore, when R_y is constant, C_R is linearly related to the maximum ductility demand μ. This observation indicates the validity of C_R as a damage indicator when SDOF systems are considered. Other damage indices based on energy criteria and/or residual displacements could have also been adopted. However, such parameters present shortcomings, e.g. require calibration, depend on the hysteretic properties and, thus, their popularity does not compare to that of maximum ductility and C_R.

Table 1
The 40 near-field records adopted.

Year	NGA	Event/station	Component	M_w	Mech.	R_{rup}	T_p (s)	D_{5-95} (s)
1971	77	San Fernando/Pacoima Dam (upper left abut)	PUL254	6.61	R	1.8	1.6	7.1
1979	150	Coyote Lake/Gilroy Array #6	GO6230	5.74	SS	3.1	1.2	3.4
1979	158	Imperial Valley-06/Aeropuerto Mexicali	AEP045	6.53	SS	0.3	2.4	7.1
1979	159	Imperial Valley-06/Agrarias	AGR273	6.53	SS	0.7	2.3	11.5
1979	170	Imperial Valley-06/EC County Center FF	ECC002	6.53	SS	7.3	4.5	14.9
1979	173	Imperial Valley-06/El Centro Array #10	E10050	6.53	SS	6.2	4.5	13.0
1979	179	Imperial Valley-06/El Centro Array #4	E04140	6.53	SS	7.0	4.6	10.2
1979	180	Imperial Valley-06/El Centro Array #5	E05230	6.53	SS	4.0	4	9.4
1979	181	Imperial Valley-06/El Centro Array #6	E06230	6.53	SS	1.4	3.8	8.5
1979	182	Imperial Valley-06/El Centro Array #7	E07230	6.53	SS	0.6	4.2	4.8
1979	183	Imperial Valley-06/El Centro Array #8	E08230	6.53	SS	3.9	5.4	5.8
1979	184	Imperial Valley-06/El Centro Differential Array	EDA270	6.53	SS	5.1	5.9	6.9
1979	185	Imperial Valley-06/Holtville Post Office	HVP315	6.53	SS	7.7	4.8	11.8
1980	292	Irpinia-Italy-01/Sturno	STU000	6.90	N	10.8	3.1	16.6
1980	250	Mammoth Lakes-06/Long Valley Dam	LUL000	5.94	SS	16.5	1.1	7.2
1981	316	Westmorland/Parachute Test Site	PTS315	5.90	SS	6.2	3.6	17.3
1983	407	Coalinga-05/Oil City	OLC270	5.77	R	2.4	0.69	2.8
1983	415	Coalinga-05/Transmitter Hill	TSM270	5.77	R	9.5	0.92	3.9
1984	451	Morgan Hill/Coyote Lake Dam (SW Abut)	CYC285	6.19	SS	0.5	0.95	3.1
1984	459	Morgan Hill/Gilroy Array #6	GO6090	6.19	SS	9.9	1.2	6.9
1986	529	N. Palm Springs/North Palm Springs	NPS210	6.06	RO	4.0	1.4	4.5
1986	568	San Salvador/Geotech Investig. Center	GIC090	5.21	SS	6.3	0.86	3.8
1987	615	Whittier Narrows-01/Downey – Co Maint Bldg	DWN180	5.99	RO	20.8	0.79	8.1
1987	645	Whittier Narrows-01/LB – Orange Ave	OR2010	5.99	RO	24.5	0.95	8.3
1987	721	Superstition Hills-02/El Centro Imp. Co. Cent	ICC090	6.54	SS	18.2	2.4	18.8
1987	723	Superstition Hills-02/Parachute Test Site	PTS225	6.54	SS	0.9	2.3	10.5
1989	738	Loma Prieta/Alameda Naval Air Stn Hanger	NAS180	6.93	RO	71.0	2	6.0
1989	802	Loma Prieta/Saratoga-Aloha Ave	STG090	6.93	RO	8.5	4.5	8.4
1992	821	Erzincan-Turkey/Erzincan	ERZ-NS	6.69	SS	4.4	2.7	6.9
1992	828	Cape Mendocino/Petrolia	PET090	7.01	R	8.2	3	16.2
1992	879	Landers/Lucerne	LCN260	7.28	SS	2.2	5.1	12.9
1994	1063	Northridge-01/Rinaldi Receiving Sta	RRS228	6.69	R	6.5	1.2	7.1
1994	1086	Northridge-01/Sylmar Olive View Med FF	SYL360	6.69	R	5.3	3.1	5.8
1995	1106	Kobe, Japan/KJMA	KJM000	6.9	SS	1.0	1.0	9.6
1999	1176	Kocaeli-Turkey/Yarimca	YRT330	7.51	SS	4.8	4.5	15.4
1999	1182	Chi-Chi-Taiwan/CHY006	CHY006-N	7.62	RO	9.8	2.6	25.8
1999	1202	Chi-Chi-Taiwan/CHY035	CHY035-E	7.62	RO	12.7	1.4	28.1
1999	1503	Chi-Chi-Taiwan/TCU065	TCU065-E	7.62	RO	0.6	5.7	28.0
1999	2457	Chi-Chi-Taiwan/CHY024	CHY024-E	6.20	R	19.6	3.2	8.6
2000	1853	Yountville/Napa Fire Station #3	2016a090	5	SS	11.4	0.73	3.3

R_{rup} (km): Closest distance to rupture plane.
R: Reverse, SS: strike-slip, N: normal, RO: reverse-oblique.
T_p (s): The period of the velocity pulse.
D_{5-95} (s): Significant duration.

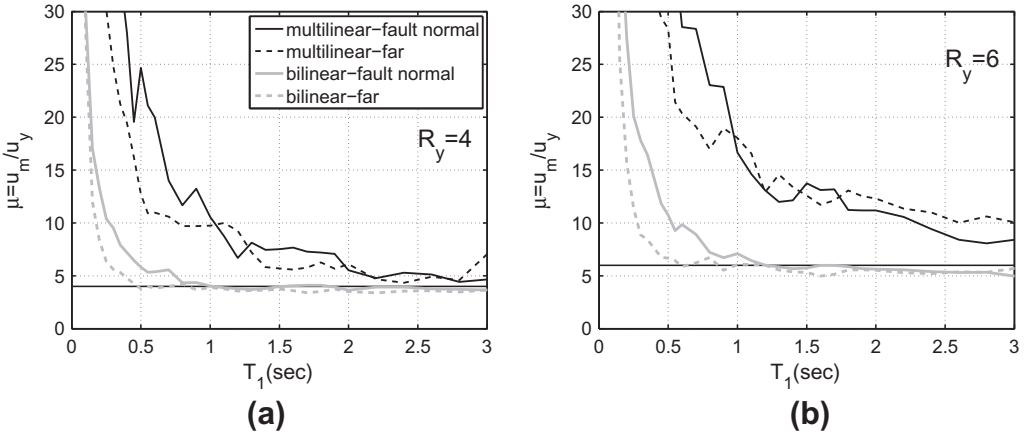

Fig. 4. Median ductility of quadrilinear and bilinear oscillators in case of pulse-type records over ordinary ground motions: (a) $R_y = 4$ and (b) $R_y = 6$.

4.1. Far versus near-field ground motions

The effect of pulse-like ground motions with respect to far-field records is studied first. Fig. 4 shows the median ductility demand of the near-field and far-field ground motions, assuming R_y equal to 4 and 6. The two sets of records are compared using the reference oscillator presented in Section 2 and the corresponding bilinear system.

Useful conclusions can be drawn from Fig. 4. It is evident that near-field records produce increased demands for periods in the vicinity of 0.5 s, for both oscillators. As the period increases this effect decays and the ductility fans around the corresponding R_y value, thus indicating that for large periods $\mu = R_y$ and $C_R = 1$. The bilinear model produces smaller ductility demands for both types of records, while all curves follow a similar degrading pattern, regardless of the considered R_y value. Moreover, for both oscillators and for the whole period range the near-field record set increased the demand compared to that of the far-field ground motions. Therefore, as shown in Fig. 4, near-field, fault normal, ground motions produce increased demands because of the velocity pulse of their fault-normal component.

4.2. The pulse period T_p

One of the key parameters, related to the rupture process of forward directivity, near-fault ground motions is the pulse period T_p. Even though the paper emphasizes on the effect of modeling and thus does not elaborate on the impact of ground motion characteristics, the pulse period is an essential parameter and its treatment may affect the findings of any similar study. Fig. 5, shows the plot of the median C_R together with its 16% and 84% fractiles versus: (a) the period (T_1) of the SDOF oscillator (Fig. 5a), and (b) the period of the SDOF oscillator normalized with respect to the pulse period (T_1/T_p) (Fig. 5b). Also, the two plots show with light gray lines the data obtained from the individual records, while the considered SDOF system is the reference oscillator with $R_y = 4$. According to Fig. 5b, normalizing the period of the oscillator leads to reduced ductility or C_R, demand, compared to the unnormalized plot of Fig. 5a. Moreover, when the period is not normalized, the dispersion is considerably larger, thus indicating that the ratio is better correlated with the demand. Therefore, despite the variability in the values of T_p, using the T_1/T_p ratio in the ordinate axis will reduce the record-to-record variability. This is also demonstrated in a later section of the paper where an MDOF building is studied.

The practice of adopting the T_1/T_p ratio instead of the system period T_1 when studding near-field ground motions, appears also in a number of past studies, e.g. [6,17–20]. Moreover, Baker and Cornell [18] suggest that pulse-type records can be classified as "aggressive" or "benign", depending on whether the ratio T_1/T_p is greater or smaller than one, respectively. Although the T_1/T_p ratio cannot be considered able to provide adequate characterization of the ground motion [17], this is another indication of its importance. Also, Mavroeidis et al. [17] claim that the normalization makes feasible the specification of design spectra and reduction factors appropriate for near-fault ground motions, while Ibarra and Krawinkler [6] use the same normalization in order to present their results when near-field ground motions are considered.

Another issue related to the pulse period T_p is the way that it is specified. Despite the many different opinions, the most common approach is assuming T_p equal to the predominant period of the velocity spectrum, i.e. the period where the velocity spectrum takes its maximum value. This approach yields accurate estimations for most cases, since in the case of fault-normal ground motions the shear waves propagate in a way that the predominant period of the Fourier acceleration spectrum, and thus the period of the corresponding velocity spectrum, is very close to the actual pulse period. Alternatively, one may use the approach proposed by Baker [21], in which using wavelet analysis, one is able to extract the largest velocity pulse from a given ground motion. The pulse period extracted from the velocity spectrum is associated, in general, with a high-frequency oscillatory portion of the ground motion, whereas the pulse extracted with wavelet analysis is associated with the main velocity pulse. The limitation of processing velocity records with wavelet analysis is that one can only extract the visible main velocity pulse, but not shorter duration distinguishable pulses that may override the long-duration near-source pulse. The periods obtained using the wavelet-based approach are, in general, larger than these obtained using the velocity spectrum. Finally, several empirical expressions, relating T_p to the moment magnitude (M_w) of the earthquake may be found in the literature (e.g. [17,22]). These relationships are valid only in an average sense and when the actual ground motion record is available, they can be used as a "simple check" of the results obtained with the methods discussed above. In our study, the classification of the records and the pulse period (T_p), were taken from the PEER NGA database.

4.3. Influence of the parameters that describe the oscillator

4.3.1. Influence of the hardening slope (a_h)

In order to obtain the reference structure the backbone parameters a_h, a_c, μ_c, r are set equal to 5%, −50%, 2 and 20% (Fig. 3c), respectively. Subsequently, every parameter is varied one at a time to study the sensitivity of the demand, assumed with the aid of the inelastic displacement ratio C_R. The period of the oscillator is normalized with the pulse period T_p, as discussed previously.

The influence of the hardening slope a_h is studied using two quadrilinear oscillators with $\mu_c = 2$ and $\mu_c = 4$. Two distinct values of μ_c are chosen in order to show the interplay of a_h with μ_c. The remaining parameters of the oscillator backbone are set equal to those of the reference system (Fig. 3c). Median C_R values are shown in Figs. 6 and 7. To help interpreting Figs. 6 and 7, we also show in Figs. 8 and 9 the corresponding hysteretic plots using the CHY006 record, see Table 1, for $T_1/T_p = 0.45$.

According to Figs. 6 and 7, the inelastic displacement ratio decreases exponentially as the normalized period T_1/T_p increases

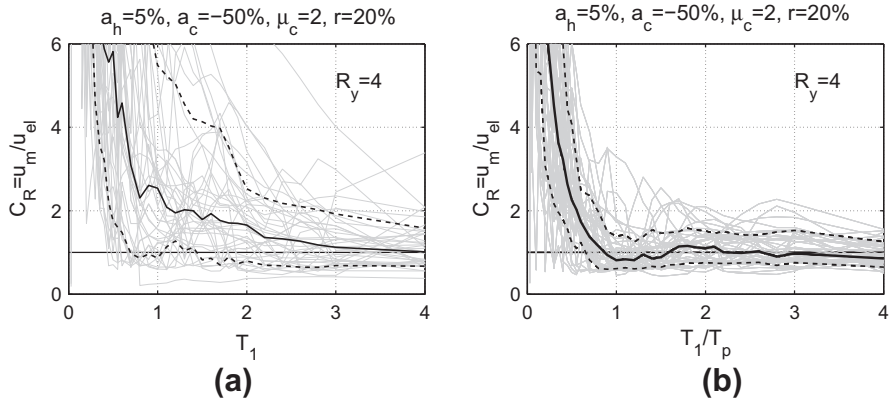

Fig. 5. Reference oscillator ($R_y = 4$): C_R ratio values versus (a) oscillator period T_1 and (b) oscillator period normalized with the pulse period T_1/T_p.

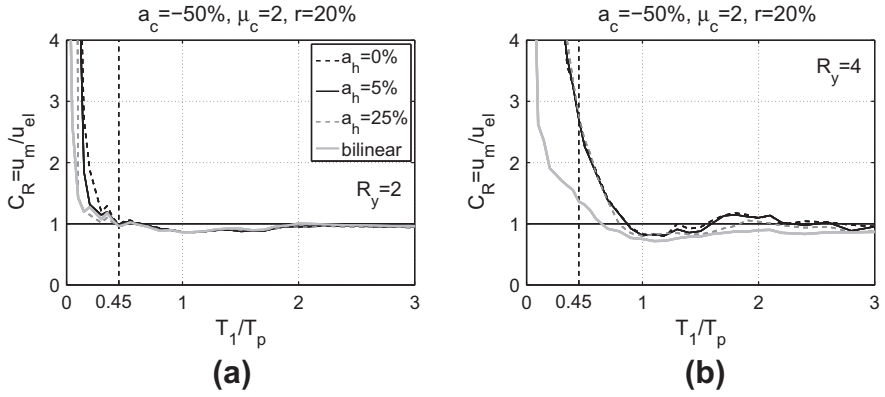

Fig. 6. Influence of the hardening slope (a_h) on C_R assuming $\mu_c = 2$: (a) $R_y = 2$ and (b) $R_y = 4$.

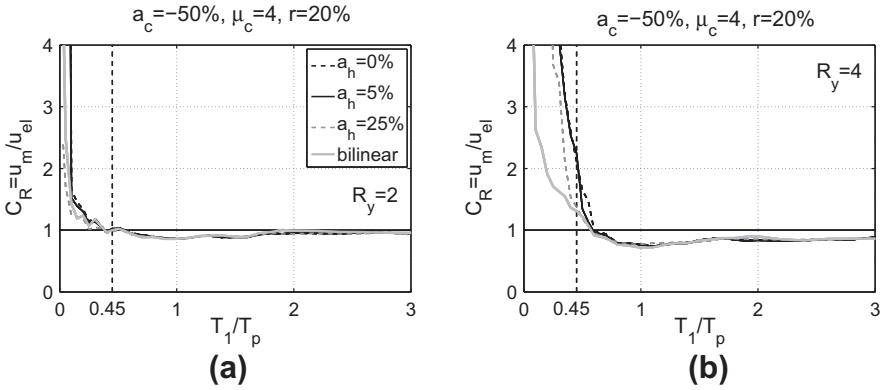

Fig. 7. Influence of the hardening slope (a_h) on C_R assuming $\mu_c = 4$: (a) $R_y = 2$ and (b) $R_y = 4$.

(Figs. 6 and 7). This pattern is in agreement with the relationship of Newmark and Hall [17]. Moreover, the ductility and also the displacement demand, follow the same trend with C_R, since $\mu = C_R R_y$ and R_y is constant. Regardless of the value of μ_c, when $R_y = 2$, the effect of a_h appears to be practically negligible, with only some minor differences for small values of T_1/T_p. This is attributed to the fact that for $R_y = 2$ and $T_1/T_p > 0.1$ the response is quite close to the elastic case, since the oscillator does not enter well into the inelastic region and the hysteresis is performed in the pre-fracturing range ($\mu < \mu_c$), as shown in the hysteretic plots of Figs. 8a and 9a.

For systems with $R_y = 4$ (Figs. 6b, 7b), the bilinear oscillator underestimates C_R over the whole period range for both μ_c values considered, while the corresponding curves follow a similar degrading pattern. For all the systems examined, as the hardening slope a_h increases, the response is underestimated compared to that of smaller a_h values. These differences can be understood by studying the hysteretic behavior of the systems of Figs. 8 and 9, although the observations made cannot be generalized for the entire period range and for every record. For $R_y = 4$ and $\mu_c = 2$ (Fig. 8b) a part of the hysteresis is evaluated beyond the capping point entering the residual segment and resulting to displacements approximately 10 times the yield displacement. This justifies why usually these systems are insensitive to the variations of a_h and why, in general, the response predicted by the bilinear system differs considerably. On the other hand, a μ_c value equal to 4 will not allow entering the post-capping region and will result to smaller C_R demands. Therefore, depending on the period of the system,

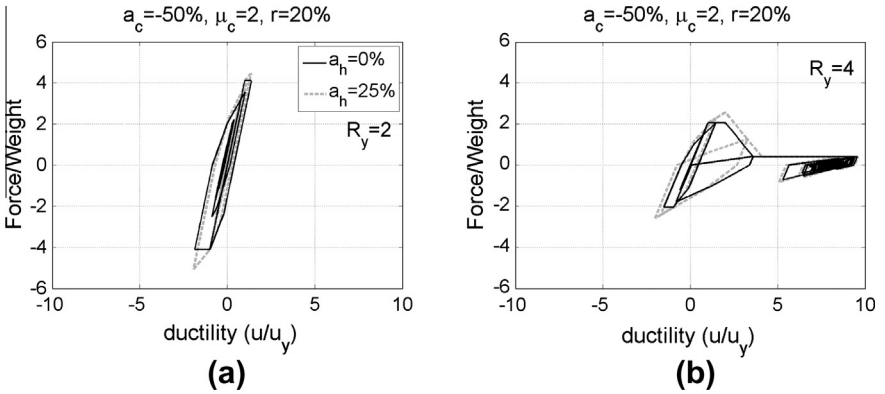

Fig. 8. Hysteretic plots of the reference oscillator ($\mu_c = 2$) and $T_1/T_p = 0.45$: (a) $R_y = 2$ and (b) $R_y = 4$.

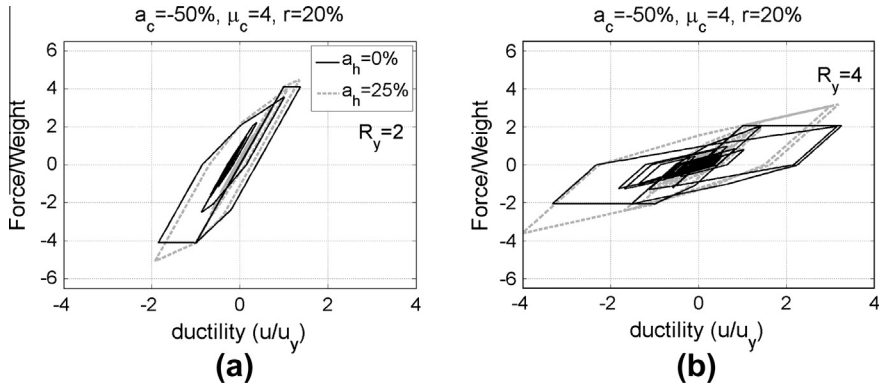

Fig. 9. Hysteretic plots of the oscillator with $\mu_c = 4$ and $T_1/T_p = 0.45$: (a) $R_y = 2$ and (b) $R_y = 4$.

a_h has some effect on C_R, while the estimates of the bilinear model in the second case are sufficient.

Another useful observation is that the T_1/T_p value where the descending branch approaches almost asymptotically the $C_R = 1$ horizontal line (Figs. 6 and 7) depends on R_y. As R_y increases, the threshold is shifted to the right, and is not sensitive to a_h and μ_c. In a later section it is shown that the location of this point is controlled primarily by the residual capacity of the system, r. In all, near-field ground motions induce large inelastic displacements compared to the far-field case and thus the effect of the a_h–μ_c interplay will be more pronounced. Trends similar to $R_y = 4$ are expected as R_y increases, e.g. for $R_y = 6$ and 8.

4.3.2. Influence of the post-capping slope (a_c)

Contrary to the small effect of a_h, the post-capping slope a_c is expected to have a more pronounced effect as has been identified for the far-field case [6].

Fig. 10 shows the inelastic displacement ratio versus T_1/T_p for four different levels of the strength reduction factor ($R_y = 2$, 4, 6 and 8). In order to better understand the results of Fig. 10, we also show the hysteretic plot obtained with the CHY006 record (Table 1) when $T_1/T_p = 0.45$ (Fig. 11). According to Fig. 10a, for systems with R_y equal to 2, the differences in C_R appear in the initial normalized period range ($T_1/T_p < 0.2$) where the response is very close to that of the bilinear case. The $a_c = -200\%$ case is the only exception, since for a small R_y (e.g. $R_y = 2$) a very steep slope ($a_c = -200\%$) is able to differentiates the response from the bilinear case. For larger T_1/T_p values (e.g. $T_1/T_p > 0.45$) the response of all systems is identical (Fig. 10a). Moreover, for all the R_y values considered, the difference from the bilinear case becomes distinct and increases as the slope becomes steeper and R_y increases. The differences can be explained by the hysteretic plots of Fig. 11c and d.

Differences are also observed for large T_1/T_p values ($T_1/T_p \geqslant 1$) for $R_y = 4$ and 6. Thus, the influence of the post-capping slope on

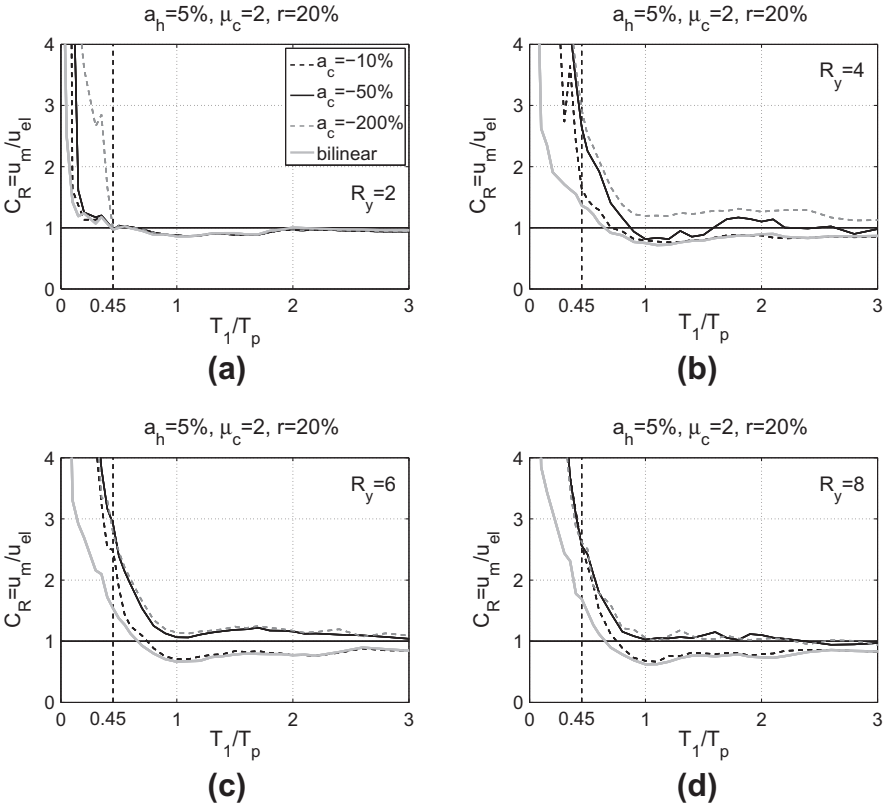

Fig. 10. Influence of the post-capping slope (a_c) on C_R: (a) $R_y = 2$, (b) $R_y = 4$, (c) $R_y = 6$ and (d) $R_y = 8$.

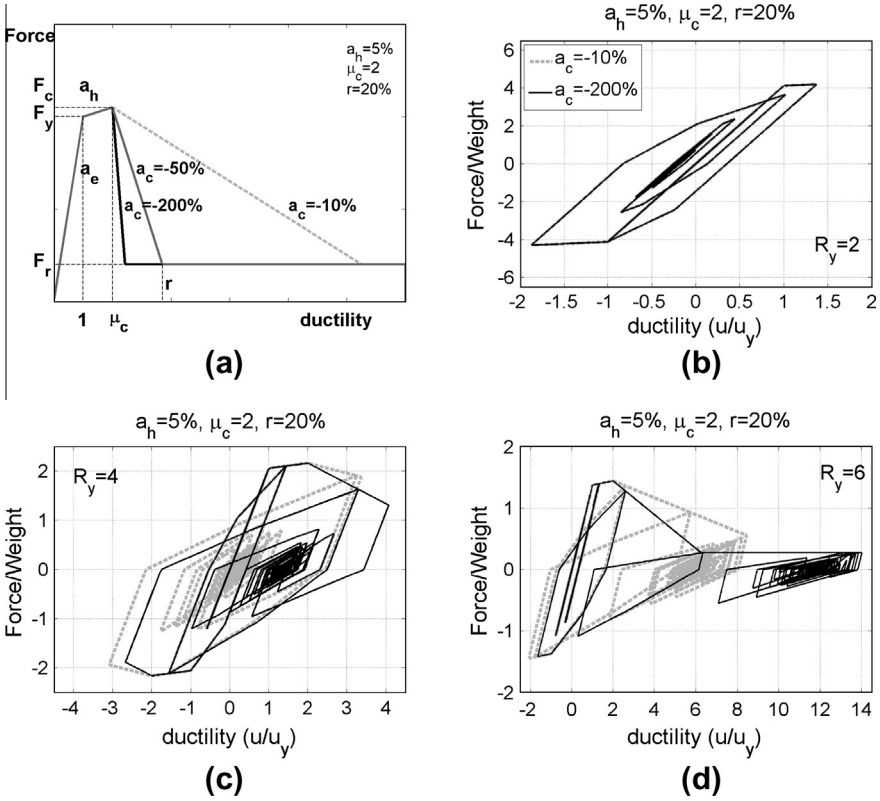

Fig. 11. (a) Backbone curve for the a_c values equal to −10%, −50% and −200% and, hysteretic plots for T_1/T_p = 0.45, and (b) R_y = 2, (c) R_y = 4, (d) R_y = 6.

the seismic response is greatly affected by the examined R_y level. Depending on R_y, the maximum displacement demand may occur in: (a) the initial elastic branch, (b) the descending branch, or (c) ultimately, the horizontal residual segment (Fig. 2). According to the results of Fig. 11, every case will affect in a different way the hysteretic behavior. When the hysteresis is performed in the post-capping branch (Fig. 11c), the variations in a_c will have a more pronounced effect; thus, justifying the increased differences observed (e.g. Fig. 10b).

Although not shown in the plots, it is noted that the effect of the negative slope a_c is amplified by the level of the residual strength, r, and the capping ductility μ_c. Increasing μ_c is expected to highly affect inelastic systems (e.g. R_y = 8), while increasing the residual strength r will reduce the sensitivity of the response to variations of a_c. Finally, C_R was found to be insensitive to variations of a_c in the −25% to −10% and the −200% to −100% range.

4.3.3. Influence of the capping ductility (μ_c)

Fig. 12 shows the influence of the capping ductility μ_c. The effect of this parameter has been already discussed when studying the effect of a_h. Therefore, when varying μ_c, the overall shape of the curves remains similar to that of the a_c, as shown in Fig. 10. The value of μ_c will accelerate or delay the onset of the capping point (the point that degradation starts) and will differentiate the response from the bilinear case. Hence, for low R_y levels only oscillators with small μ_c ductility, i.e. μ_c = 1.2, are affected as shown in Fig. 12a, while as the capping ductility increases the response approaches that of the bilinear system, especially for T_1/T_p beyond 0.5. Although not shown here, again the interplay of the oscillator parameters are important, e.g., for systems with either less steep post-capping slope (a_c) or larger residual strength (r) the effect of μ_c on C_R is expected to decrease.

4.3.4. Influence of the residual strength (r)

Fig. 13 shows the sensitivity of the response to the residual capacity r. This parameter becomes significant for large ductility demands and especially for small values of the capping ductility μ_c. For smaller ductility demands, r will practically have no effect. Therefore, for R_y = 2, all curves coincide with the bilinear model. Moreover, very large values, e.g. r = 80%, will practically cancel out this parameter and the overall response will approach the one of the bilinear system, as seen in Fig. 13 for all R_y values. Typically, for structural problems large r, e.g. r = 80%, are not realistic and small values (e.g. r = 10% or 20%) should be expected. As R_y increases, e.g. R_y = 6 and 8, the C_R demand also increases. As before, for T_1/T_p > 1 the C_R stabilizes approximately around 1.5 for r = 5%, while a moderate r = 20% results to C_R = 1.

4.3.5. Influence of the fracturing ductility (μ_f)

All models studied throughout this paper have infinite ductility capacity, or, in other words, the horizontal residual plateau of Fig. 2 does not have a ductility upper limit. Fig. 14 shows the effect of assuming an upper limit using the μ_f parameter discussed in Section 2 and shown with a vertical dashed line in Fig. 2. This parameter can be used to model the sudden fracturing of the system or to set an upper bound to the monotonic backbone. This practice will avoid possible unrealistic values, but may introduce numerical instability. Fig. 14 shows the median inelastic deformation ratio C_R of one bilinear and two quadrilinear systems, one with infinite μ_f ductility and the another with μ_f = 10. The remaining properties of the oscillator are that of the reference oscillator. By definition $C_R = \mu/R_y$ and therefore oscillators with constant R_y have an upper bound on C_R equal to μ_f/R_y. This is verified by the findings of Fig. 14 where introducing μ_f results to upper bounds equal to 5, 2.5, 1.67 and 1.25 for R_y equal to 2, 4, 6 and 8, respectively. This bound is valid for T_1/T_p ratios less than 0.7. As clearly shown in

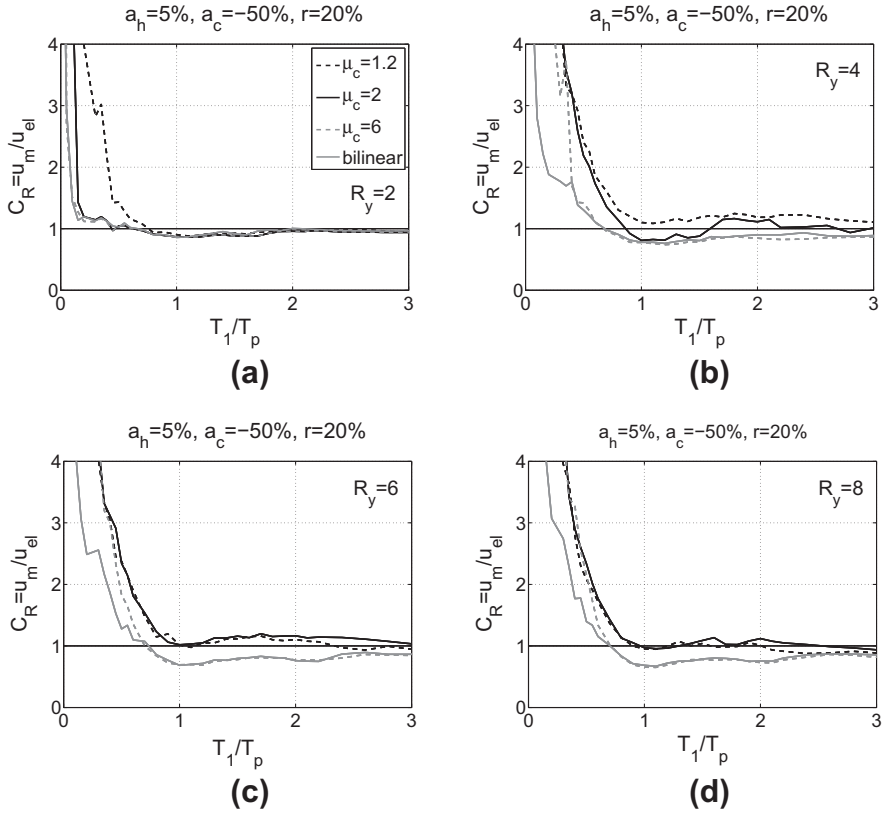

Fig. 12. Influence of the capping ductility (μ_c) on C_R: (a) $R_y = 2$, (b) $R_y = 4$, (c) $R_y = 6$ and (d) $R_y = 8$.

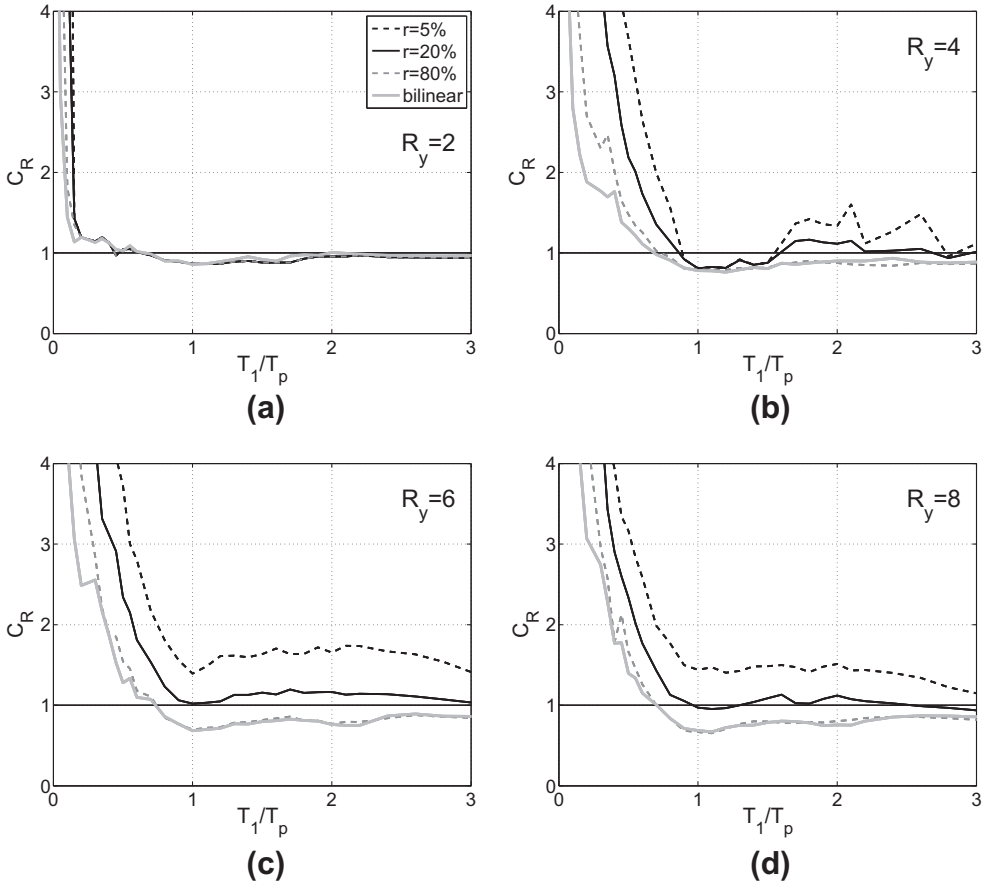

Fig. 13. Influence of the residual strength (r) on C_R: (a) $R_y = 2$, (b) $R_y = 4$, (c) $R_y = 6$ and (d) $R_y = 8$.

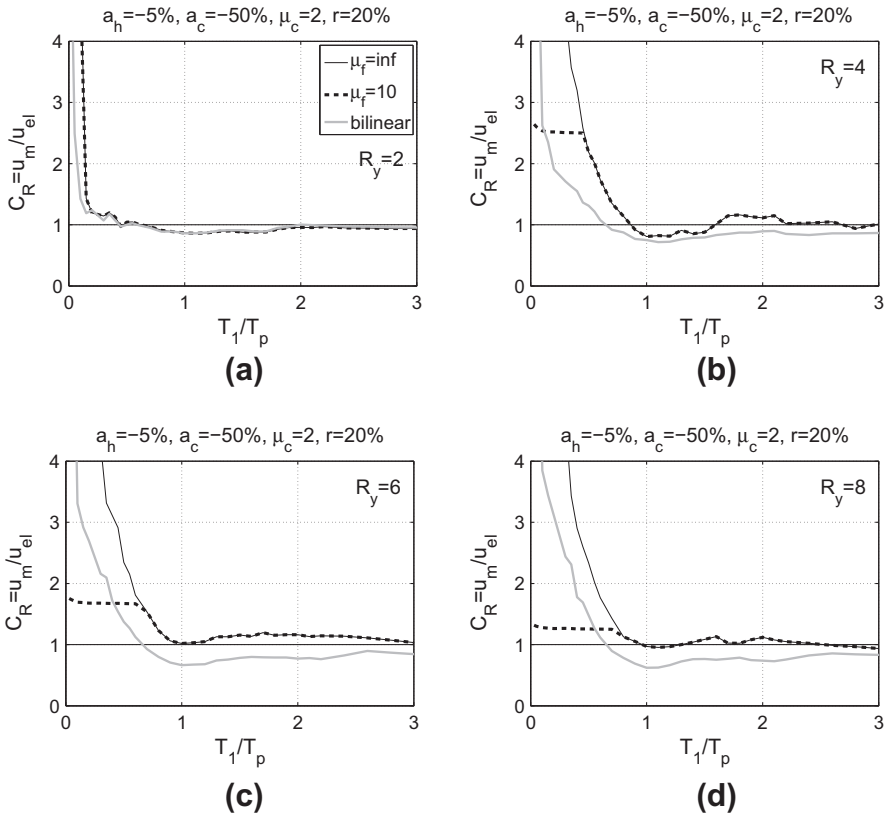

Fig. 14. The effect of the fracturing ductility (μ_f) on C_R: (a) R_y = 2, (b) R_y = 4, (c) R_y = 6 and (d) R_y = 8.

Fig. 14, the response of all quadrilinear oscillators coincide beyond the limit T_1/T_p = 0.7.

4.4. Influence of the cyclic properties

Although focus is given on the monotonic properties of the degrading oscillator (in-cycle degradation), the parameters that define the cyclic degradation are also important. The cyclic response is based on the "hysteric material" available in the material library of OpenSees [14]. The "pinchX" and "pinchY" parameters that define the pinching factor for forces and displacements, respectively, was set throughout this study equal to a moderate value of 0.5. Damage caused by energy and ductility was not considered. In general, the selection of values for the pinching parameter is possible only at the member level by calibrating the model with data available from experimental tests. For SDOF systems that refer to the building level the model can be calibrated using MDOF building models. In this study a moderate pinching value, equal to 0.5 has been selected.

Fig. 15 depicts the influence of the pinching parameter allowing comparison of the response of the reference oscillator for pinching values equal to 0.5 and 5 and R_y levels equal to 4 and 6. It can be noticed that the pinching parameter has a small effect on the median C_R demand, for both R_y values shown. This effect is practically negligible for $T_1/T_p < 1.5$, while a minor effect appears beyond this value. The small sensitivity is attributed to the properties of the incipient ground motion. When pulse-type records are considered, the seismic energy arrives in a few large pulses that contain the cumulative effect of almost all seismic energy. Therefore, because of the small number of strong cycles, the effect of the pinching parameter is expected to be small compared to longer records with more cycles.

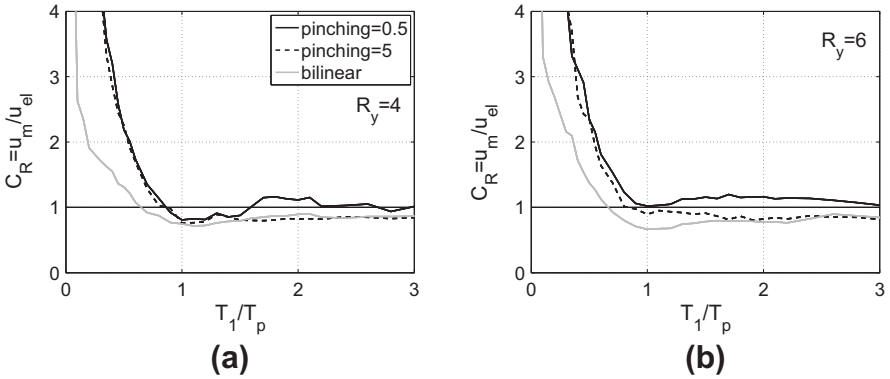

Fig. 15. The effect of the pinching parameter on C_R: (a) R_y = 4 and (b) R_y = 6.

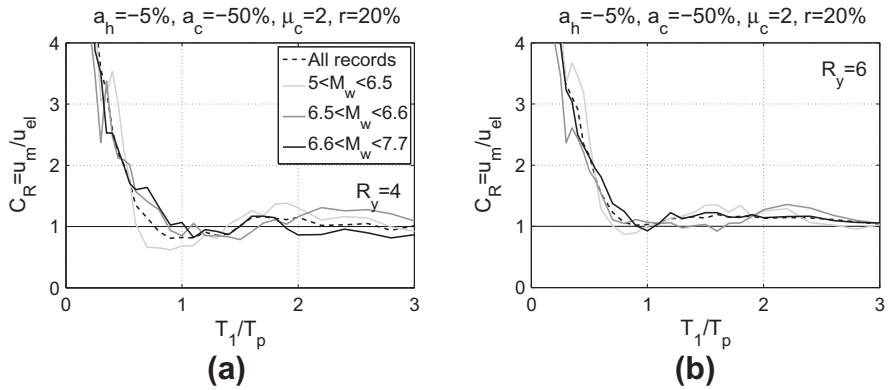

Fig. 16. Median C_R of quadrilinear oscillators for the forward-directivity near-field ground motion with respect to M_w, (a) $R_y = 4$ versus T_1/T_p and (b) $R_y = 6$ versus T_1/T_p.

4.5. Sensitivity to magnitude, pulse period and fault mechanism

Apart from the properties of the model, the ground motion properties may influence the demand when near-field ground motions are considered. For the sake of completeness a quick examination of these effects is attempted, although it is not in the scope of paper. Focus is given on the magnitude, the pulse period and the fault mechanism. According to [23] the peak ground velocity (PGV) may also influence C_R, although in [19] it is suggested that neither PGV nor the distance to the source significantly affect C_R. Thus, the latter parameters were not considered.

Among the parameters that characterize near-field ground motions, the magnitude (M_w) and the pulse period (T_p) seem to be the most influential. Consensus among researcher exists on the fact that the pulse period increases with magnitude. This is attributed to the physics of the fault rupture and is expressed with a linear relationship between the logarithm of the pulse period and the magnitude. For example, Rupakhety et al. [24] propose the formula:

$$\log_{10} T_p = -2.87 + 0.47 M_w \quad (2)$$

Thus, according to Eq. (2), T_p and M_w are collinear and therefore their effect on C_R is expected to follow a similar pattern. However, we create groups separately for M_w and T_p, since the pulse period is directly correlated with the magnitude only in an average sense, while large scatter can be found when using such an assumption in conjunction with Eq. (2). For example, for some records of Table 1 (records with NGA numbers 316, 2457, 821) T_p is not always positively correlated to M_w. Therefore, the 40 near-field ground motions of Table 1 are grouped to three sets with magnitudes (M_w) in the ranges 5–6.5, 6.5–6.6 and 6.6–7.7. Three sets were also formed with respect to T_p. The sets are chosen so that they contain approximately the same number of records with respect to M_w and T_p.

Fig. 16 shows the effect of the magnitude M_w for the three sets considered. The median of the whole ground motion database is also shown. As shown in Fig. 16a and b, when varying the T_1/T_p, the earthquake magnitude does not have a clear impact on the response. This is not the case when the period is not normalized with the period of the pulse as shown in Fig 17a and b. In the latter case, the minimum C_R demand corresponds to the minimum M_w value, while the largest C_R demand corresponds to moderate earthquake magnitudes. This trend has been reported by other researchers in the past [25]. According to our plots, if the fundamental period of the oscillator is normalized with the pulse period, only some minor differences can be seen for $R_y = 4$. In this case the differences are well-distributed over the whole period range, but since no clear trends can be identified, they should be considered as statistically insignificant. This is in agreement with findings of other researchers [17,19] that have reported the moderate influence of earthquake magnitude in the response when the oscillator period is normalized with respect to the pulse period.

Fig. 18 shows the plots of C_R, when the records of Table 1 are grouped with respect to the pulse period. As the grouping based on M_w, it is difficult to identify clear trends and therefore the effect of T_p seems small provided that we have normalized the oscillator period with T_p. More specifically, for $T_1/T_p < 0.2$, where the spectral acceleration is constant, the response appears similar for all three groups and both R_y values, indicating that the pulse effect is lost in the high frequency portion of the ground motion. For $T_1/T_p > 1$, the normalized response is not influenced by the input excitation and the equal displacement rule applies ($C_R = 1$).

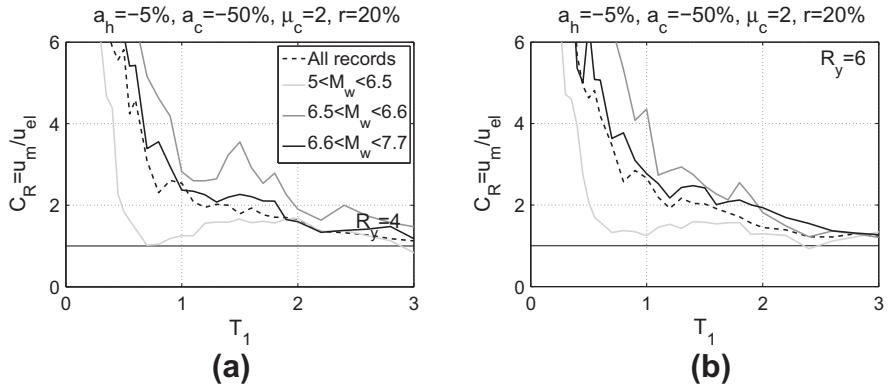

Fig. 17. Median C_R of quadrilinear oscillators for the forward-directivity near-field ground motion with respect to M_w, (a) $R_y = 4$ versus T_1 and (b) $R_y = 6$ versus T_1.

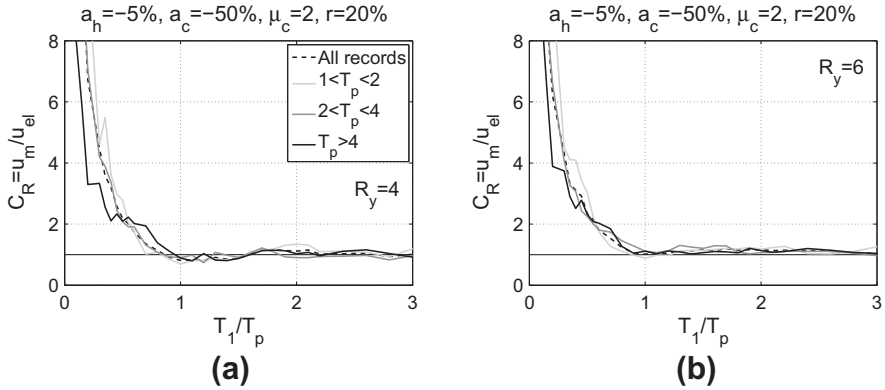

Fig. 18. Median C_R for the forward-directivity records with respect to T_p: (a) $R_y = 4$ and (b) $R_y = 6$.

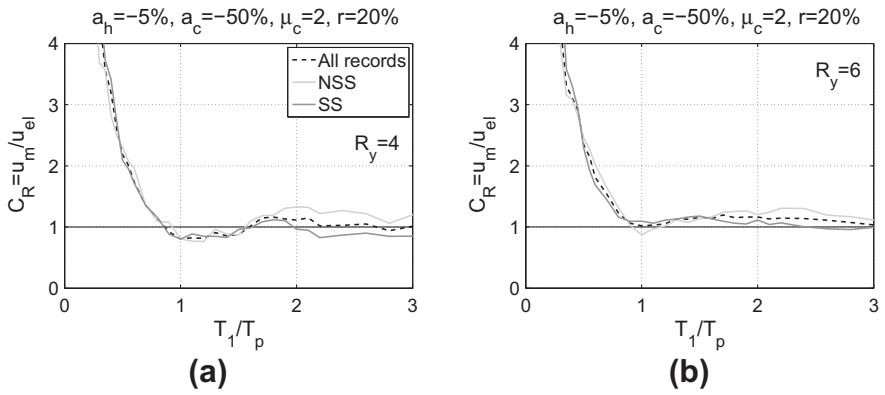

Fig. 19. The effect of fault mechanism of median C_R demand (NSS: non-strike-slip, SS: strike slip): (a) $R_y = 4$ and (b) $R_y = 6$.

The fault mechanism is another parameter that was examined. Two bins of strike-slip and non-strike-slip ground motions were formed. The non-strike slip set includes records that are reverse, normal and reverse oblique. According to Fig. 19 insignificant differences are observed for T_1/T_p values less 2, and a small effect appears as the ratio becomes larger. However, even if the response is not influenced by the mechanism, this observation cannot exclude the possible influence of the factors that characterize both strike-slip and non-strike-slip events, as discussed in Somerville et al. [22].

5. Extension to multi-degree-of-freedom structures

A nine-story steel moment-resisting frame is adopted in order to extend the discussion to a real-scale structure. The purpose is to demonstrate that the observations made regarding the response of SDOF systems can be extended to MDOF buildings. More specifically, it is shown that for near-field ground motions, and especially for degrading systems, the use of equivalent SDOF systems and of the C_R values already discussed, will improve considerably the estimation of the MDOF displacements, needed for design and assessment. The C_R estimate for structures located in the near-fault zone has been previously examined [4,17,19,23,24], studied as bilinear systems.

The building shown in Fig. 20 is a nine-story steel moment resisting frame, designed according to the 1997 NEHRP provisions. This is a peripheral frame that has five bays and a hinge-story basement. Its geometry and member sections are shown in Fig. 20. The gravity loads and the mass of the internal gravity-resisting frames are placed on a leaning column, which does not contribute to the lateral stiffness. The fundamental period of the frame is $T_1 = 2.35$ s and the mass modal participation of the first mode amounts to 84% of the total mass. Thus, the frame is essentially dominated by the first mode. A centerline model is formed using the OpenSees platform [14]. The model is able to explicitly account for the geometric nonlinearities in the form of P–Δ effects. The columns are assumed linear-elastic, while a quadrilinear model is adopted for the beam–column connections. The backbone of the moment–rotation relationship is based on a model similar to the force–deformation relationship of the SDOF systems that follows the backbone of Fig. 2. More specifically, the moment–rotation relationships have properties equal to $a_h = 10\%$, $a_c = -50\%$, $\mu_c = 3$, $r = 50\%$, values that are kept constant for the whole building.

In order to obtain the building's capacity curve, static pushover analysis was performed using a lateral load pattern based on the first-mode. The static pushover capacity curve is shown in Fig. 21. Because of the fracturing of the beam-column connections, the pushover curve follows a degrading pattern similar to that of the SDOF oscillators previously studied. This similarity allows to directly expand the SDOF discussion to MDOF buildings provided that we have first obtained the corresponding equivalent SDOF (ESDOF) system. Therefore, the pushover capacity curve is approximated with a trilinear curve, as shown in Fig. 21. The properties of the ESDOF system are obtained from the expressions:

$$F_y^{ESDOF} = F_y^{MDOF}/M_1^* \tag{3}$$

$$D_y^{ESDOF} = D_y^{MDOF}/\Gamma_1 \tag{4}$$

where M_1^* and Γ_1 are the generalized mass and the modal participation factor of the first mode, respectively, and F_y^{MDOF}, D_y^{MDOF} are obtained from the trilinear approximation of the pushover curve

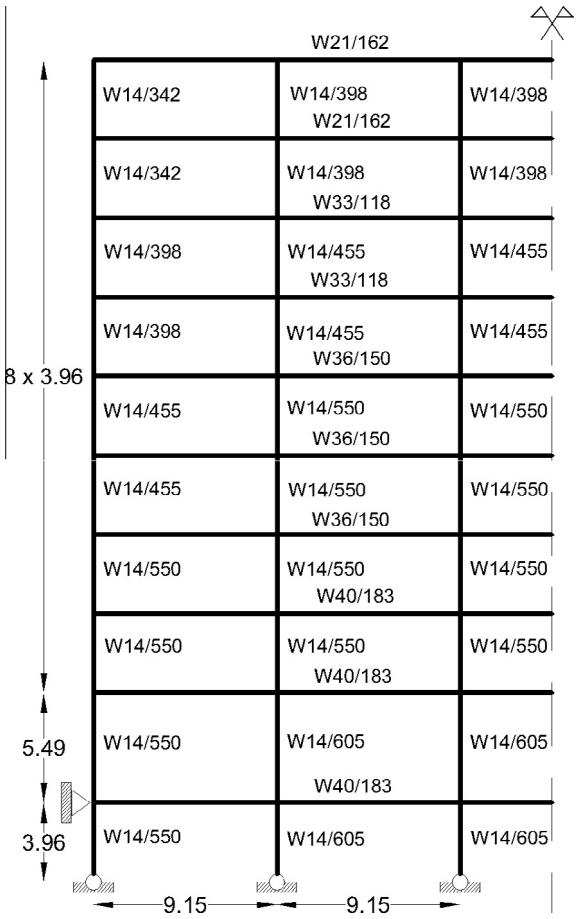

Fig. 20. The nine-story steel moment-resisting frame.

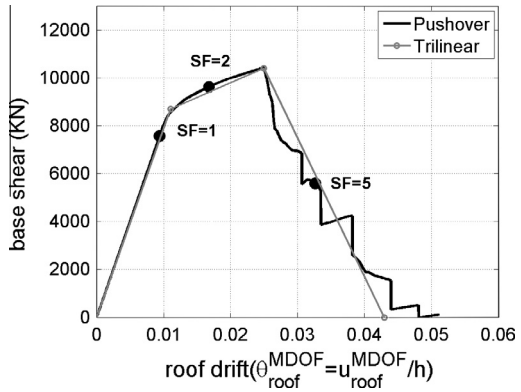

Fig. 21. Pushover capacity curve of the nine-story steel building and its trilinear approximation.

(Fig. 20). Having approximated the capacity, the properties of the ESDOF were found equal to: $a_h = 15\%$, $a_c = -30\%$, $\mu_c = 2.3$ and $r = 0\%$. When nonlinear response history analysis is performed, the displacement of the MDOF can be obtained from the mean displacement of the ESDOF as $u^{MDOF} = \Gamma_1 u^{ESDOF}$.

Nonlinear response history analysis of the nine-story structure is performed using a degrading multilinear and a bilinear ESDOF oscillator, considering both far and near-field motions. Every ground motion set is scaled to its median spectral velocity that corresponds to the fundamental period of the building. The pulse-type set the records were again scaled using uniform scale factors equal to 1, 2 and 5. The first scale factor corresponds to nearly-elastic behavior, while the scale factors equal to 2 and 5 correspond to inelastic behavior with different ductility demands. The mean displacements caused by the three scaled ground motion sets are shown in the static pushover curve of Fig. 21. For the far-field records the three scale factors were chosen in order to result in displacements of the MDOF system similar to those of the pulse type records. Therefore, the scale factors of the far-field set were considered equal to 1.3, 2.7 and 6.5.

In earthquake engineering practice it is necessary to estimate the displacement demand in order to design and/or assess the capacity of a building. For this purpose, various R_y–C_1–T (or R_y–μ–T) predicting relationships have been proposed. Practically, the majority of R–C_1–T relationships follow a format similar to that of the early Newmark–Hall relationship [17]. Moreover, during design and assessment a common approach to determine the displacement demand is through the ASCE/SEI 41-06 [27] formula. According to this formula, the target displacement is calculated from:

$$u = C_o C_1 C_2 S_a \frac{T_e^2}{4\pi^2} \tag{5}$$

where C_o is a factor used to equate the displacement a SDOF system with the displacement of the actual building and is usually assumed equal to Γ_1, the participation factor of the first mode. C_1 is the inelastic displacement ratio obtained from either pertinent R_y–C_1–T relationships or tabulated values [27]. C_2 is a factor to consider pinching hysteresis and cyclic strength degradation and T_e is the effective first mode period. As an obvious improvement of Eq. (5), one can replace C_1 with C_R, as discussed in the previous sections.

Fig. 22 shows the mean and the standard deviation of the displacement estimated using nonlinear response history analyses (NRHA) for both far and pulse-type ground motions. Moreover, the plots show the estimation obtained using the ASCE/SEI 41-06 formula (Eq. (5)) and the expression proposed in [4]. According to Fig. 21, similar trends can be observed for both pulse-type and far-field records. The direct determination of the target displacement using the modified ASCE/SEI 41-06 [26] relationship provides improved demand estimates only for low scale factors that correspond to either linear or nearly elastic response. As the intensity increases and the system starts to behave nonlinearly, the ASCE/SEI 41-06 [26] approach systematically overestimates the demand for the MDOF structure. The same results are obtained if Eq. (5) is applied using the C_R value obtained from the relationship of Ref. [4]. Both models give worse predictions for the far-field ground motion set, compared to the near-field case. On the other hand, for every scale factor the displacement estimate of the degrading ESDOF is close to that of the MDOF structure. The bilinear ESDOF can approximate the response of the MDOF only up to the capping point. These findings are in agreement with the results presented in the NIST 2010 [27] document. It should be pointed out that our findings cannot be directly expanded to all MDOF systems; it would be beneficial to study a series of buildings of different heights and plans in order to deduce general conclusions. Such an analysis is outside the scope of the present study. Moreover, our findings are valid only in an average sense, since individual ground motions can always produce peak values that considerably differ from the mean.

It would also be interesting to investigate the effect of the T_1/T_p ratio on the prediction of the ESDOF. According to Baker and Cornell [18], pulse-type records can be separated to either "aggressive" or "benign", depending on whether the ratio T_1/T_p is above or below one, i.e. the pulse period is larger or smaller than the fundamental period of the system. Therefore, they classify records with $T_1/T_p < 1/2$ and $2 > T_1/T_p > 2/3$ as "aggressive" and "benign", respectively.

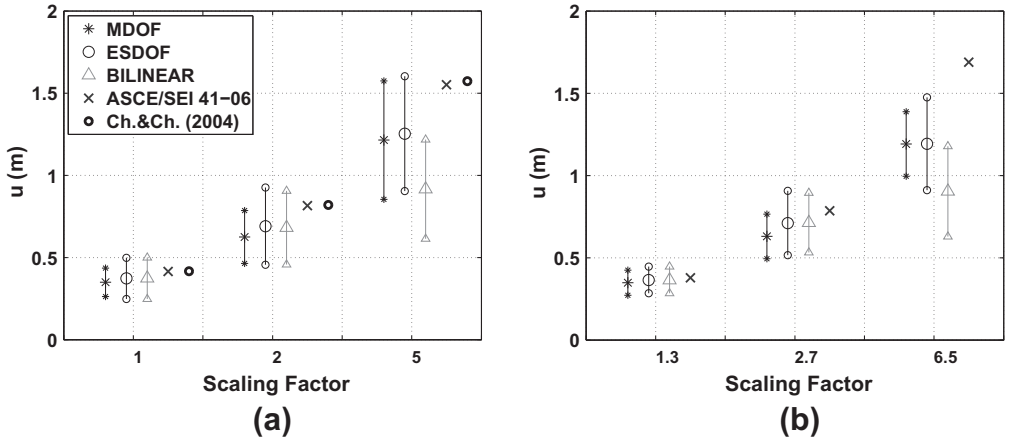

Fig. 22. Peak roof displacement for (a) pulse-type and (b) far-field ground motions.

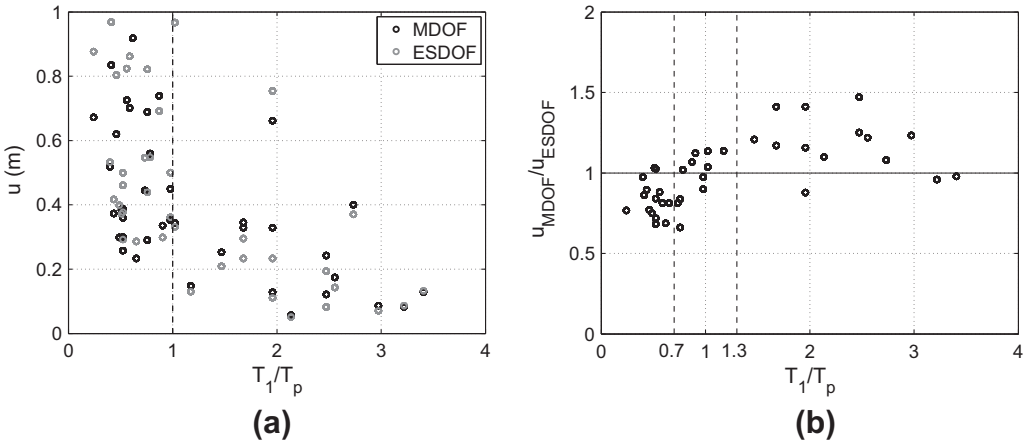

Fig. 23. (a) Maximum top displacement of MDOF and ESDOF systems and (b) Ratio of the computed displacements of the MDOF system over the corresponding estimates of the ESDOF.

According to Fig. 23a, records with $T_1/T_p < 1$ produce increased inelastic displacement demands compared to the $T_1/T_p > 1$ case for both MDOF and ESDOF systems. This verifies the distinction between aggressive and benign records for this building; however, one must bear in mind that this classification should be handled with caution as there will be cases that it may not be strictly true. Moreover, according to Fig. 23b, for records with pulses shorter than the fundamental period of the building the ESDOF overestimate the displacements and the opposite occurs when $T_1/T_p > 1$. This implies that for $T_1/T_p > 1$, the higher modes have a significant contribution, while for longer pulses ($T_1/T_p < 1$) their effect is small. Again this observation holds for the building studied and thus, caution is required before generalizing.

6. Conclusions

A series of SDOF systems with different properties has been subjected to a set of near-field ground motions in order to investigate the effect of modeling on degrading systems. It is demonstrated that the oscillator backbone has a significant effect on the seismic response. The inelastic displacement ratio (C_R) values computed for fault-normal records are usually higher than those of far-field excitations. Moreover, it is shown that non-degrading bilinear models may consistently underestimate the C_R demand compared to models with degrading properties. This is why most R_y–μ–T relationships cannot be directly applied to degrading systems under forward-directivity records, especially for large displacement/ductility demands. The selected sample of representative near-field records demonstrates that magnitude and rupture mechanism has a minor effect. Considering quadrilinear oscillators, the relationship between the peak deformation of the inelastic and the corresponding linear SDOF systems is greatly affected by the four parameters that describe the backbone of the oscillator. Among the four parameters considered, the normalized height of the residual plateau r was found to be the most influential parameter, for almost all periods and regardless of the level of R_y-demand. However, the response was also sensitive to the combinations of the four parameters, especially to the combination of capping ductility μ_c and to the residual capacity r. A nine-story steel frame was also investigated and trends similar to the SDOF case were identified. For the examined MDOF structure, the displacement coefficient approach of ASCE/SEI 41-06 is efficient only for relatively small, elastic and nearly-elastic displacements, while an appropriate C_R or ESDOF system should be used when a large displacement demand is expected.

References

[1] Bertero VV, Mahin SA, Herrera RA. A seismic design implication of near-fault San Fernando earthquake records. Earthquake Eng Struct Dynam 1978;6: 31–42.

[2] Hall JF, Heaton TH, Halling MW, Wald DJ. Near-source ground motions and its effects on flexible buildings. Earthquake Spectra 1995;11(4):569–605.

[3] Alavi B, Krawinkler H. Effects of near fault ground motions on frame structures. Report no. 138. The John A. Blume Earthquake Engineering Center, Department of Civil and Environmental Engineering, Stanford University; 2001.

[4] Chopra AK, Chintanapakdee C. Inelastic deformation ratios for design and evaluation of structures: single-degree-of-freedom bilinear systems. J Struct Eng 2004;130:1309–19.

[5] Spyrakos C, Maniatakis Ch, Taflambas J. Evaluation of near source seismic records based on damage potential parameters. Case study: Greece. Soil Dynam Earthquake Eng 2008;28:738–53.

[6] Ibarra L, Krawinkler H. Global collapse of frame structures under seismic excitations. Report no. 152. The John A. Blume Earthquake Engineering Center, Department of Civil and Environmental Engineering, Stanford University; 2005.

[7] Ibarra L, Medina R, Krawinkler H. Hysteretic models that incorporate strength and stiffness deterioration. Earthquake Eng Struct Dynam 2005;34:1489–511.

[8] Lignos DG, Krawinkler H. Deterioration modeling of steel components in support of collapse prediction of steel moment frames under earthquake loading. J Struct Eng 2011;137:1291–302.

[9] Fragiadakis M, Vamvatsikos D. Fast performance uncertainty estimation via pushover and approximate IDA. Earthquake Eng Struct Dynam 2010;39: 683–703.

[10] Sezen H. Evaluation and testing of existing reinforced concrete building columns. Report CE299. University of California, Berkeley; 2000.

[11] Inoue K, Asari T, Ishiyama Y. Lateral stiffness-strength distribution and damage concentration along the height of a building. In: The 12th world conference on earthquake engineering, Upper Hutt, New Zealand, January 30–February 4; 2000.

[12] Elwood K. Shake table tests and analytical studies on the gravity load collapse of reinforced concrete frames. PhD dissertation. Department of Civil and Environmental Engineering, University of California, Berkeley; 2002.

[13] Haselton C, Deierlein G. Assessing seismic collapse safety of modern reinforced concrete frame. PEER report 2007/08. Pacific Engineering Research Center, University of California, Berkeley, California; 2007.

[14] Mazzoni S, McKenna F, Scott MH, Fenves GL. OPENSEES, OpenSees command language manual. Open system for earthquake engineering simulation; 2011.

[15] Quantification of building seismic performance factors and commentary for the seismic rehabilitation of buildings (FEMA P695). Report, prepared by the Applied Technology Council for the Federal Emergency Management Agency, Washington, DC; 2009.

[16] Newmark NM, Hall WJ. Earthquake spectra and design. Berkeley: Earthquake Engineering Research Center, University of California; 1982.

[17] Mavroeidis GP, Dong G, Papageorgiou AS. Near-fault ground motions, and the response of elastic and inelastic single-degree-of-freedom (SDOF) systems. Earthquake Eng Struct Dynam 2004;33:1023–49.

[18] Baker JW, Cornell CA. Vector-valued intensity measures for pulse-like near-fault ground motions. Eng Struct 2008;30:1048–57.

[19] Ruiz-García J. Inelastic displacement ratios for seismic assessment of structures subjected to forward-directivity near-fault ground motions. J Earthquake Eng 2011;15:449–68.

[20] Iervolino I, Chioccarelli E, Baltzopoulos G. Inelastic displacement ratio of near-source pulse-like ground motions. Short Communication, Earthquake Eng Struct Dynam; 2012. <http://wileyonlinelibrary.com>. http://dx.doi.org/10.1002/eqe.2167 [published online in Wiley Online Library].

[21] Baker JW. Quantitative classification of near-fault ground motions using wavelet analysis. Bull Seismol Soc Am 2007;97:1486–501.

[22] Somerville PG, Smith NF, Graves RW, Abrahamson NA. Modification of empirical strong motion attenuation relations to include the amplitude and duration effects of rupture directivity. Seismol Res Lett 1997;68(1): 199–222.

[23] Báez JI, Miranda E. Amplification factors to estimate inelastic displacement demands for the design of structures in the near field. In: The 12th world conference on earthquake engineering, Upper Hutt, New Zealand, January 30–February 4; 2000.

[24] Rupakhety R, Sigurdsson SU, Papageorgiou AS, Sigbjörnsson R. Quantification of ground-motion parameters and response spectra in the near-fault region. Bull Earthquake Eng 2011;9:893–930.

[25] Somerville P. Magnitude scaling of the near-fault rupture directivity pulse. Phys Earth Planet Inter 2003;137:201–12.

[26] Seismic rehabilitation of existing buildings. Reston (VA). American Society of Civil Engineers, ASCE/SEI 41-06; 2006.

[27] NIST. Applicability of nonlinear multiple-degree-of-freedom modeling for design. Report no. NIST GCR 10-917-9. Prepared for the US National Institute of Standards and Technology by the NEHRP Consultants Joint Venture, Gaithersburg, MD; 2010.